Angular distribution of sputtered particles and surface morphology: the case of beryllium under a krypton beam at various incidences

P.-G. Fournier [a,*], A. Nourtier [b], V.I. Shulga [c], M. Ait El Fqih [a,d]

[a] Laboratoire de Spectroscopie de Translation des Interactions Moléculaires, Université Paris-Sud, Bât. 478, Orsay 91405, France
[b] Laboratoire de Physique des Solides, Université Paris-Sud, Bât. 510, Orsay 91405, France
[c] Institute of Nuclear Physics, Moscow State University, 119992 Moscow, Russian Federation
[d] SIAM-MEC, Faculté des Sciences, Université Cadi Ayyad, Semlalia, B.P. 2390, Marrakech, Morocco

Abstract

A beryllium target is bombarded with 5 keV krypton ions at incidence angles of 0° and 70°. The sputtered material is collected on a Mylar cylindrical foil surrounding the target, the foil is cut into pieces and the deposit on them is measured by inductively coupled plasma optical emission spectroscopy (ICP-OES). Experiment is combined with simulations using the computer code OKSANA. The method supplies accurate angular distributions of sputtered particles. The surface morphology is observed by scanning electron micrography. Depending on the incidence angle, sputtering forms craters and rippled areas or deep grooves. The resulting differences between simulations and experiment are explained qualitatively.
© 2004 Elsevier B.V. All rights reserved.

1. Introduction

Ion beam sputtering [1–3] is primarily characterised by the total yield Y. A deeper insight into the ejection process is supplied by the energy and angular distribution of ejected particles. As regards the angular distribution, a simple and accurate method to obtain it has been described recently [4,5]: a Mylar foil is used as a collector, the deposit is analysed by inductively coupled plasma optical emission spectroscopy (ICP-OES), numerical simulations complete the treatment. Here the method is applied to polycrystalline

---
* Corresponding author. Tel.: +33 6 60 65 74 86; fax: +33 1 69 15 75 76.

   E-mail address: paul-guy.fournier@stim.u-psud.fr (P.-G. Fournier).

beryllium. Beryllium is a metal of technological interest for plasma devices, which has motivated studies of its sputtering by light projectiles (D, He, Be) [6–8]. In the present case the projectiles are krypton ions. Experiments were made at four angles of incidence, 0°, 30°, 70° and 80°. Only the results at 0° and 70° are reported here. In fact the results at 30° are close to those at 0° and those at 80° close to those at 70°.

2. Method

The sputtering device is the same as in earlier studies of optical emissions [9–11]. A horizontal beam of 5 keV krypton ions hits the vertical surface of the sample under an angle of incidence α (see Fig. 1). The background pressure is less than 0.5×10^{-8} Torr without the beam, about 10^{-8} Torr with the beam on. In order to collect the sputtered particles, a polyethylene terephthalate (Mylar™) foil is rolled upon a vertical cylinder of radius R whose axis passes through the impact spot. A point (x, y) of the foil is thus seen from the spot under angles $\lambda = \arctan(y/R)$ from the incidence plane and $\mu = x/R$ in it from the normal. The radius R is 21.8 mm in the experiments at $\alpha = 0°$, 30° and 80°, and 50 mm in the experi-

ment at $\alpha = 70°$. After sputtering, the foil is removed and pieces are cut out. The cutting layout is a compromise between resolution requirements and a reasonable number of measurements. The smallest pieces are squares of 25 mm^2 for $\alpha = 0°$ and rectangles of 50 mm^2 for $\alpha = 70°$, forming series along horizontal or vertical directions. The rest of the foil is cut into pieces of larger area. The deposit on every piece is dissolved in concentrated acid, the solution is diluted and analysed by ICP-OES. Two different apparatus are used. Their respective accuracy is limited to 2% and 10% by calibration and to 2.5% and 9% by stability.

The simulations are done with the well-tested computer code OKSANA [12–14]. The polycrystalline target is modelled by a single crystal of random orientation. Its temperature is 300 K. The heat of sublimation of Be (3.38 eV) is used for the planar surface barrier. The interatomic potential is the standard WHB (KrC) potential [15]. In order to test a possible effect of atomic roughness, simulations are done with either a perfect surface or a surface embodying 50% vacancies in the first monolayer. Furthermore for oblique incidence both the WHB potential and the so-called "universal" ZBL potential [16] are tried. As will be seen (Figs. 2, 4 and 5), the differences between the
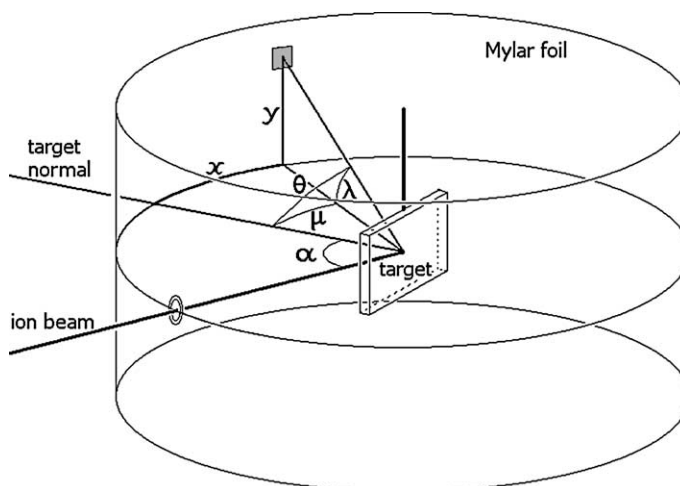
Fig. 1. Experimental scheme.
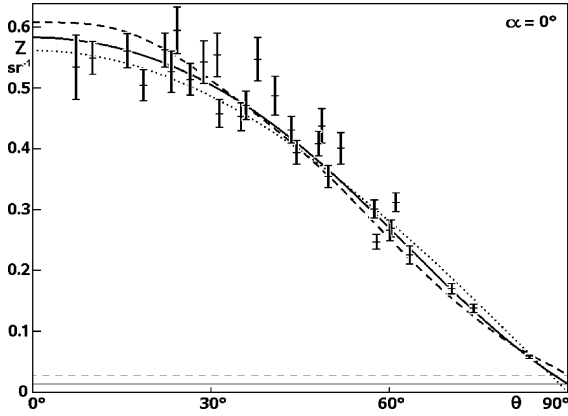
Fig. 2. Differential sputtering yield per solid angle Z as a function of polar angle θ. *Experiment* ($Z = Z_i^{\exp}$, $\theta = \theta_i$): crosses with error bars. *Simulations* ($Z = fZ^{\sim} + g$): dashes (WHB potential and no vacancy), solid line (WHB potential and 50% vacancies); the line at the bottom is the isotropic contribution g. *Cosine law* (adjusted with $g = 0$): dots.

various simulations are less than their differences from the experiments. A simulation is stopped when the number of ejected atoms reaches 500 000. Excepted in very low flux directions, the statistical error is less than the difference between simulations. In the special case $\alpha = 0°$ where the symmetry of revolution around the normal is used, the statistical error is negligible.

The physical quantity which best characterises the angular distribution is the differential sputtering yield per solid angle $Z = dY/d\Omega$. In practice the deposit is measured on a surface i seen from the impact spot under a finite solid angle Ω_i. The deposit is converted into a partial sputtering yield $Y_i^{\exp}$ or an average differential sputtering yield per solid angle $Z_i^{\exp} = Y_i^{\exp}/\Omega_i$, then compared with the result of the simulations for the same solid angle $Z_i^{\sim} = Y_i^{\sim}/\Omega_i$. This conversion implies that all the particles that income onto the collector stick on it, which has been proven elsewhere [4,5].

Experiment is subject to two kinds of uncertainties, random (mainly due to ICP stability) and systematic (due to ion current and ICP calibrations). In order to get rid of the second ones and concentrate on the profile of the angular distribution, a normalisation procedure is applied. A linear relationship is assumed:

$$Z_i^{\exp} \approx fZ_i^{\sim} + g,$$

f and g are calculated by minimising the χ^2:

$$\chi^2 = \sum_i \left(Z_i^{\exp} - fZ_i^{\sim} - g\right)^2 / \left(\sigma_i^2 + f^2\tau_i^2\right),$$

where σ_i^2 is the variance of $Z_i^{\exp}$ due to random uncertainties and τ_i^2 that of $Z_i^{\sim}$ due to statistics, knowing that in a simulation the variance of the number of particles emitted within a given solid angle is this number itself. The isotropic background g is expected to be small. It is introduced because a deposit is obtained not only on the half-cylinder facing the target, but also on surfaces in the shadow of it, as seen in Fig. 4 for $\mu > 90°$. Its origin is discussed in [5]. Once f and g are known, the best estimate for the (experimental) total sputtering yield is

$$Y^{\exp} = fY^{\sim} + 4\pi g.$$

3. Results at normal incidence

In the experiment at $\alpha = 0°$ the target is bombarded for 59 h with a beam of intensity 2.1 μA and cross section 0.95 mm^2, giving a fluence of 2.9×10^{18} ions/mm^2. The simulations give $Y^{\sim} = 1.2$ whether the first monolayer embodies vacancies or not. The fitting procedure gives:

- no vacancy: $f = 1.31$; $g = 0.03$; $Y^{\exp} = 1.9$;
- 50% vacancies: $f = 1.39$; $g = 0.01$; $Y^{\exp} = 1.8$.

$Y^{\exp}$ is thus 50% larger than $Y^{\sim}$. From $Y^{\exp}$ one deduces a mean erosion rate of 2.05 Å/s and a mean erosion depth of 44 μm, which is compatible with a maximum erosion depth of 210 μm as measured by scanning electron microscopy.

Owing to the axial symmetry, the appropriate variable is the polar angle θ. For a finite surface an average angle θ_i is defined by

$$\cos\theta_i = \frac{1}{\Omega_i} \int_{\Omega_i} \cos\theta \, d\Omega.$$

With this definition a cosine law ($Z \propto \cos\theta$) would be correctly rendered ($Z_i \propto \cos\theta_i$) whatever the surface size is.

Fig. 2 displays the results, as well as a cosine law for comparison. The two simulated profiles
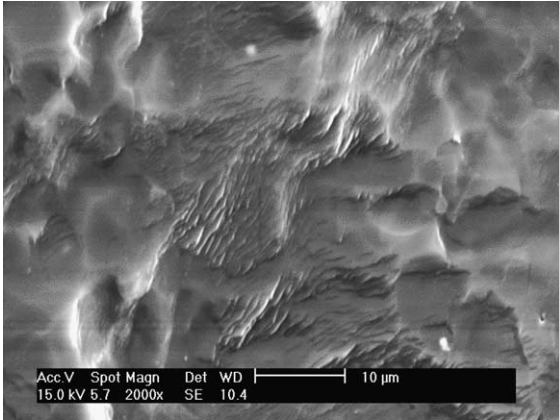
Fig. 3. A typical micrograph of the surface after bombardment at normal incidence.

are slightly overcosine, but the experiment does not share this feature. The differences are most marked in the range $20° < \theta < 50°$. The origin of the discrepancies can be understood by considering scanning electron micrographs of the bombarded surface (see Fig. 3). They reveal craters of typical size 10 μm intertwined with rippled areas. Ripples are known [17,18] to rise in the first stage of sputtering, then to give place to kinetic roughening with a growing roughness height. The influence of roughness on the sputtering yield is primarily through the distribution of slopes. As far as these are weak ($<30°$), the local angular distribution of sputtered particles is close to cosine and so is the average one, since the average of randomly tilted cosine distributions is cosine. When the slopes are strong the distribution of sputtered particles is locally shifted towards the reflected direction, so that the average distribution has a maximum at non-zero θ. Here the slopes evaluated by scanning electron microscopy range from zero to high values (60° and more). This explains the flattening of the observed distribution in Fig. 2 for $\theta < 30°$.

4. Results at oblique incidence

In the experiment at $\alpha = 70°$ the target is bombarded for 92 h with a beam of intensity 0.69 μA and cross section 1.25 mm^2, giving a fluence of

0.38×10^{18} ions/mm^2. The foil is cut into 70 pieces. The simulations use a WHB potential and a first monolayer with 0% or 50% vacancies or a ZBL potential and no vacancy. The fitting procedure gives:

- WHB, 0%: $Y^{sim} = 10.2$; $f = 0.91$; $g = 0.037$;
- WHB, 50%: $Y^{sim} = 10.0$; $f = 0.93$; $g = 0.036$;
- ZBL: $Y^{sim} = 10.8$; $f = 0.86$; $g = 0.037$.

In the three cases $Y^{exp} = 9.8 \pm 0.9$, compatibly with Y^{sim}. This leads to a mean erosion rate of 1.02 Å/s and a mean erosion depth of 34 μm, which is compatible with a maximum erosion depth of 140 μm as measured by scanning electron microscopy.

Figs. 4 and 5 display the angular profile for two selected sets of pieces, 23 along the x-axis, 13 along the y-axis. As at normal incidence, the simulations are close to each other. The experiment shows some differences with them, which are much more marked along the y-axis (Fig. 5) than the x-axis (Fig. 4). Scanning electron micrographs of the surface (see Fig. 6) reveal grooves parallel to the plane of incidence, with typical period and height of 10 μm, a typical length of 100 μm and sharp ends facing the incoming ion flux. Inside a groove smaller grooves appear at various scales. Thus unlike
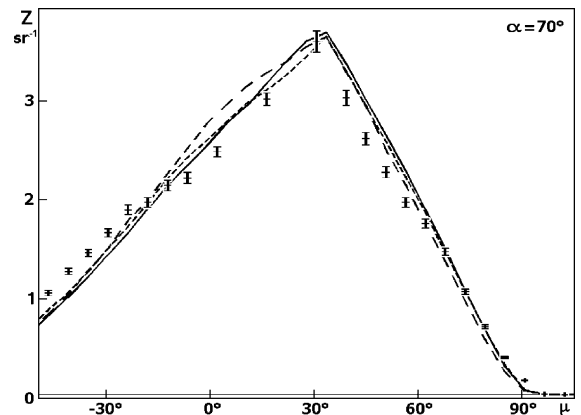
Fig. 4. Differential sputtering yield per solid angle Z for a series of surfaces along the x-axis as a function of angle μ at the centre of the surface. *Experiment* ($Z = Z_i^{exp}$): crosses with error bars. *Simulations* ($Z = fZ_i^{sim} + g$): long dashes (WHB, no vacancy), short dashes (WHB, 50% vacancies), solid line (ZBL); the line at the bottom is the isotropic contribution g. The lines are guides to the eyes.
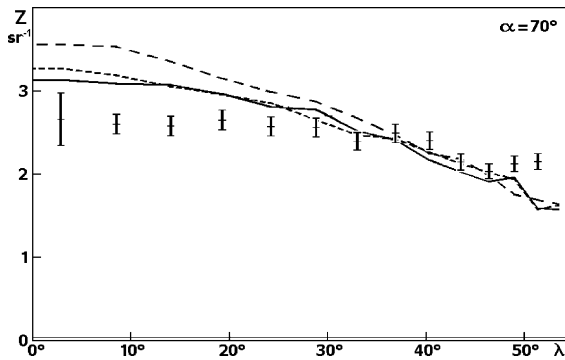
Fig. 5. Same as Fig. 4 for surfaces along the *y*-axis as a function of angle λ at the centre of the surface.
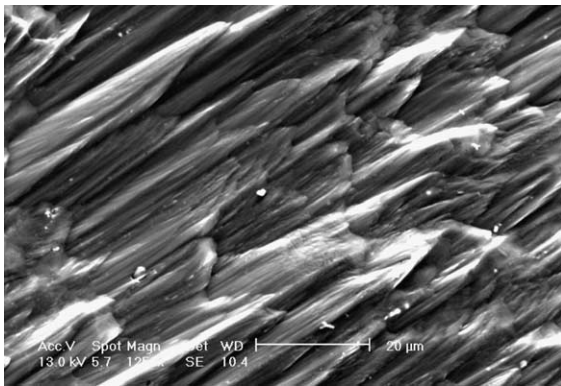
Fig. 6. A typical micrograph of the surface after bombardment at oblique incidence. Ions come from the right parallel to the grooves.

the case $\alpha = 0°$ the local normal is strongly tilted almost everywhere. Schematically the normal rocks by about 60° from one side of the incidence plane to the other. At first approximation the situation can be modelled by considering such tilted (plane) surfaces and averaging over the two directions. Preliminary calculations confirm that the angular profile along the *y*-axis is nearly flat for $\lambda < 30°$ as observed. Beyond 30°, the approximation becomes questionable owing to shadowing, reflection and re-sputtering at the microrelief.

5. Conclusion

The angularly-resolved sputtering yield of beryllium for heavy projectiles and different angles of incidence has been measured and OKSANA simulations have been used to process the data. The overall agreement is good, but a close examination reveals discrepancies that are ascribable to roughness effects. Qualitatively the distribution of slopes as shown by scanning electron microscopy explains most of the discrepancies. However several effects associated with strong roughness such as shadowing, reflection and re-sputtering would have to be included in a quantitative treatment. The sensitivity of the ICP technique makes it possible to measure much smaller deposits with practically the same accuracy. A study of the angular distribution at various stages of erosion is thus feasible.

References

[1] P. Sigmund (Ed.), Fundamental Processes in Sputtering of Atoms and Molecules, Mat. Fys. Medd. Dan. Vid. Selsk 43 (1993).
[2] G. Betz, K. Wien, Int. J. Mass Spectr. Ion Proc. 140 (1994) 1.
[3] V.I. Shulga, Nucl. Instr. and Meth. B 164–165 (2000) 733.
[4] P.-G. Fournier, O. Varenne, J. Baudon, A. Nourtier, T.R. Govers, Appl. Surf. Sci. 225 (2004) 135.
[5] P.-G. Fournier, A. Nourtier, V.I. Shulga, Phys. Chem. News 19 (2004) 60.
[6] D.N. Ruzic, P.C. Smith, R.B. Turkot Jr., J. Nucl. Mater. 241–243 (1997) 1170.
[7] P.C. Smith, D.N. Ruzic, Nucl. Fusion 38 (1998) 673.
[8] M. Küstner, W. Eckstein, E. Hechtl, J. Roth, J. Nucl. Mater. 265 (1999) 22.
[9] J. Fournier, P.-G. Fournier, A. Kaddouri, H. Dunet, J. Appl. Phys. 69 (1991) 2382.
[10] P.-G. Fournier, J. Fournier, B. Bellaoui, O. Benoist d'Azy, G. Taieb, Nucl. Instr. and Meth. B 78 (1993) 144.
[11] O. Varenne, P.-G. Fournier, J. Fournier, B. Bellaoui, A. Faké, J. Rostas, G. Taieb, Nucl. Instr. and Meth. B 171 (2000) 259.

[12] V.I. Shulga, Radiat. Eff. 70 (1983) 65.
[13] V.I. Shulga, P. Sigmund, Nucl. Instr. and Meth. B 119 (1996) 359.
[14] V.I. Shulga, W. Eckstein, Nucl. Instr. and Meth. B 145 (1998) 492.
[15] W.D. Wilson, L.G. Haggmark, J.P. Biersack, Phys. Rev. B 15 (1977) 2458.
[16] J.F. Ziegler, J.P. Biersack, U. Littmark (Eds.), The Stopping and Range of Ions in Solids, Vol. 1, Pergamon Press, New York, 1985, p. 41.
[17] D. Ghose, S.B. Karmohapatro, Adv. Electron. Electron Phys. 79 (1990) 73.
[18] M.A. Makeev, R. Cuerno, A.-L. Barabási, Nucl. Instr. and Meth. B 197 (2002) 185.